

Coupled Drift-Diffusion (DD) and Multi-Subband Boltzmann Transport Equation (MSBTE) Solver for 3D Multi-Gate Transistors

Seonghoon Jin, Sung-Min Hong[†], Woosung Choi, Keun-Ho Lee*, and Youngkwan Park*

Device Lab, Samsung Semiconductor Inc., 3655 North 1st Street, San Jose, CA, USA

[†] School of Information and Communications, GIST, Gwangju, Korea

* Semiconductor R&D center, Samsung Electronics, Hwasung-si, Gyeonggi-do, Korea

E-mail: s.jin@samsung.com

Abstract—This paper presents a self-consistent coupled DD/MSBTE solver for the device simulation of realistic 3D multi-gate transistors. The MSBTE for quasi-1D k -space is solved in the channel region while the DD equation is solved in the source/drain regions with an appropriate boundary condition at the DD/MSBTE region interfaces. In the MSBTE region, 2D Schrödinger equation with the two (electrons) or six (holes) band $k \cdot p$ Hamiltonian is solved to obtain the subband structure for arbitrary crystal orientations and stress conditions. Phonon and surface roughness scattering processes are taken into account in the MSBTE where the surface roughness scattering model has been extended to consider arbitrary cross-sections. Silicon nanowire transistors are considered as an application.

I. INTRODUCTION

For logic applications, 3D multi-gate transistors are being introduced into production due to their superior gate controllability. As the cross-sections perpendicular to the channel direction of the multi-gate transistors are typically uniform, subbands can be defined along the channel direction and semi-classical carrier transport in the subbands can be described by the MSBTE [1]. In realistic multi-gate transistors, however, the device cross-sections of the source/drain regions are quite different from the channel region, and the MSBTE cannot be applied to the entire simulation domain including the source, channel, and drain regions. To avoid this problem, this paper presents a self-consistent coupled DD/MSBTE solver for the device simulation of realistic 3D multi-gate transistors.

II. BOUNDARY CONDITIONS

In this work, the MSBTE for quasi-1D k -space [1] is solved in the channel region while the DD equation is solved in the source/drain regions. In order to provide a boundary condition for the MSBTE at the DD/MSBTE region interfaces, the quasi-Fermi potential computed from the DD equation (Φ_{DD}) is averaged at the interface cross-section ($\partial\Omega$) with the carrier density obtained from

the DD equation (n_{DD}) as a weighting factor:

$$\Phi_{\text{avg}} = \frac{\int_{\partial\Omega} \Phi_{DD}(\mathbf{r}) n_{DD}(\mathbf{r}) d\mathbf{r}}{\int_{\partial\Omega} n_{DD}(\mathbf{r}) d\mathbf{r}} \quad (1)$$

Then, the Fermi-Dirac distribution function with the computed quasi-Fermi potential Φ_{avg} is injected into the MSBTE region. On the other hand, the carrier flux computed from the MSBTE ($F_{\text{BTE}} [s^{-1}]$) enters as a boundary condition of the DD equation. Again, the carrier density from the DD equation is used as a weighting factor to compute the local flux density [$\text{cm}^{-2}\text{s}^{-1}$] from the flux across the whole cross-section:

$$\mathbf{F}_{DD}(\mathbf{r}) \cdot \mathbf{n}(\mathbf{r})|_{\partial\Omega} = F_{\text{BTE}}(z) \frac{n_{DD}(\mathbf{r})}{\int_{\partial\Omega} n_{DD}(\mathbf{r}') d\mathbf{r}'} \quad (2)$$

where \mathbf{n} is the interface normal vector.

As a result, the local carrier density is not necessarily continuous at the DD/MSBTE interface. The Poisson equation is solved in the entire DD/MSBTE regions to obtain self-consistent solutions.

III. SUBBAND AND QUANTIZATION MODELS

In the MSBTE region, 2D Schrödinger equation is solved by using the finite element method at multiple device cross-sections along the channel direction to obtain the subband structure in the 1D k -space. As for the Hamiltonian of the 2D Schrödinger equation, an ellipsoidal band model (with effective masses and band-offsets computed from the two-band $k \cdot p$ model [2]) for electrons and six-band $k \cdot p$ model for holes [3], [4] are employed to handle arbitrary crystal orientations and stress conditions. More details of our 2D Schrödinger equation solver can be found in [5].

In the DD region, the density-gradient equation [6] is solved to take into account the quantization effects.

IV. SCATTERING MODELS

As for the scattering operators, phonon and surface roughness scattering processes are considered. For the phonon scattering, conventional acoustic and optical

phonon scattering models similar to [1], [7] are considered. For holes, wavevector-dependent form factors are employed based on the initial k value as proposed in [8].

Particular attention is given to the surface roughness scattering model as we need to handle arbitrary 2D cross-sections. In addition, it is important to ensure that the calculated mobility converges to the value computed from the 2D k -space mobility calculation in the 1D quantization limits. To calculate the surface roughness scattering rate, we introduce the circumference coordinate s , the interface normal vector \mathbf{n} , and the roughness profile $\Delta_{s,z}$ as shown in Fig. 1. Then, the matrix element of the surface roughness scattering is modeled as:

$$\langle |V_{q_z; \mu\mu'}^{\text{SR}}|^2 \rangle = \sum_{n=-n_c}^{n_c} \left| \Gamma_{\mu\mu' q_s = \frac{2\pi n}{C}} \right|^2 \langle |\Delta_{q_s = \frac{2\pi n}{C}, q_z}|^2 \rangle \quad (3)$$

$$\langle |\Delta_{q_s, q_z}|^2 \rangle = \frac{\pi \Delta^2 \Lambda^2}{LC} \left[1 + \frac{\Lambda^2}{2} (q_s^2 + q_z^2) \right]^{-3/2} \quad (4)$$

$$\Gamma_{\mu\mu' q_s} = \oint_C ds \sum_{i=1}^{b_{\max}} \sum_{j=1}^{b_{\max}} \Gamma_{\mu\mu'}^{(ij)}(s) e^{iq_s s} \quad (5)$$

$$\Gamma_{\mu\mu'}^{(ij)}(s) = \frac{\Delta_{\text{ori}}}{\Delta} \left(\nabla \Psi_{\mu}^{(i)*} \cdot \mathbf{n} \right) H_{nn}^{(ij)} \left(\nabla \Psi_{\mu'}^{(j)} \cdot \mathbf{n} \right) \quad (6)$$

$$H_{nn}^{(ij)} = \sum_{\alpha=x}^y \sum_{\beta=x}^y M_{\alpha\beta}^{(ij)} n_{\alpha} n_{\beta} \quad (7)$$

where μ and μ' represent the subband indices, $q_z = k - k'$ is the 1D momentum transfer, C is the circumference of the interface, Δ is the reference rms value of roughness, Λ is the correlation length (1.2 nm for electrons, 4 nm for holes), $n_c \approx 2C / (\pi\Lambda)$, b_{\max} is the number of bands (1 for electrons, 6 for holes), $\Delta_{\text{ori}}(s)$ is the surface-orientation-dependent rms value of roughness, Ψ_{μ}^i is the wavefunction for $k = 0$, n_{α} is the α -component of \mathbf{n} , $M_{\alpha\beta}^{(ij)}$ is the coefficient of the bulk Hamiltonian as:

$$H_{\text{bulk}}^{(ij)} = M_0^{(ij)} + \sum_{\alpha=x}^z \sum_{\beta=x}^z M_{\alpha\beta}^{(ij)} k_{\alpha} k_{\beta} \quad (8)$$

Equation (3) takes into account the Prange-Nee contribution [7] for an arbitrary 2D cross-section. For electrons, we employ $\Delta_{100} = 0.4$ nm and $\Delta_{110} = 0.52$ nm. For holes, $\Delta = 0.25$ nm is used independent of surface orientations. As shown in (4), the exponential rather than the Gaussian power spectrum density is employed in this work. Please note that the hole mobility limited by surface-roughness scattering can diverge when the Gaussian power spectrum density is used.

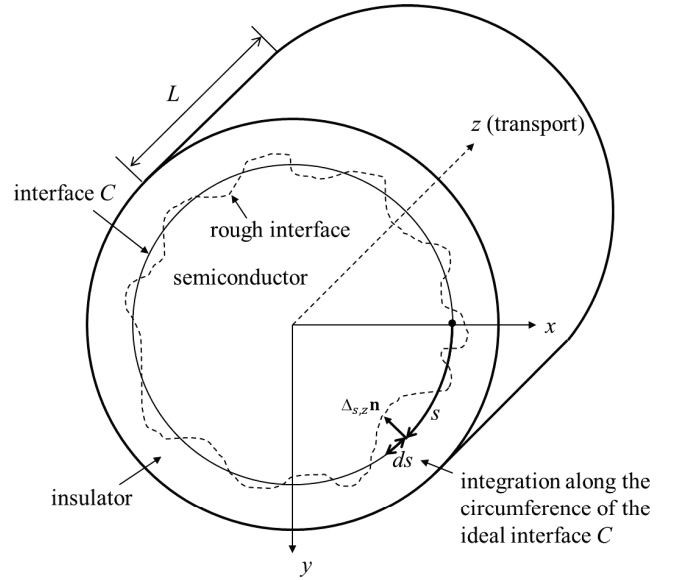


Fig. 1. Definition of circumference coordinate s , interface normal vector \mathbf{n} , and the surface roughness $\Delta_{s,z}$.

V. SIMULATION RESULTS

To check the validity of the implemented 2D Schrödinger solver in the 1D quantization limit, we first compare our results with a well-established mobility calculator Sentaurus Band [8] which computes low-field mobility based on the solution of the 1D Schrödinger equation. Fig. 2 shows the computed electron and hole mobilities at double-gate-like rectangular nanowire cross-sections with $W_{\text{Si}} = 4$ nm and $H_{\text{Si}} = 20$ nm for different surface orientations and stress conditions. While the (001) [(1 $\bar{1}$ 0)] surface exhibits higher electron (hole) mobility for the relaxed silicon, the electron (hole) mobility enhancement due to uniaxial stress is larger for the (1 $\bar{1}$ 0) [(001)] surface orientation. In addition, the computed mobility curves agree reasonably well with the results from Sentaurus Band [8] which assumes $H_{\text{Si}} \rightarrow \infty$.

In Fig. 3, the electron and hole density profiles at the cross-section for the strong inversion bias condition are shown. We also compare the carrier density at the center of the cross-section with that from Sentaurus Band in Fig. 3 (c) and (d). We obtain excellent agreement for the electron density profile. For the hole density calculation, we use the wavevector at $k = 0$ and neglect the k -dependence of the wavefunction, which may cause some differences between the two simulators especially for the case of (1 $\bar{1}$ 0) surface at 0 GP.

Near the top and bottom corners, there exist non-negligible 2D quantization effects especially for the (1 $\bar{1}$ 0) side wall nFET and the (001) side wall pFET since the quantization along the side wall is strong (in other words, the quantization mass is small). As a result, carriers are squeezed to the corners. For these surface

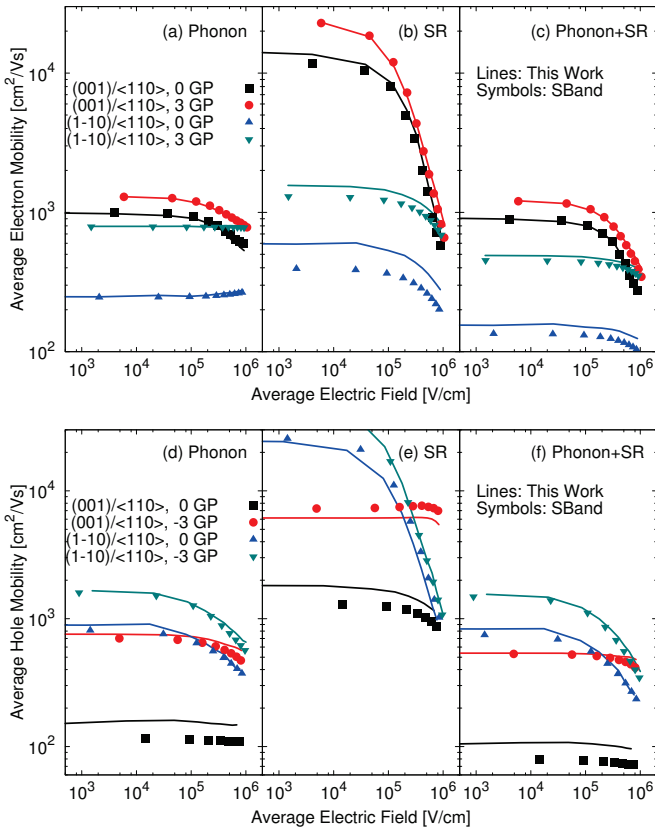


Fig. 2. Calculated electron [(a) phonon-limited, (b) SR-limited, (c) phonon+SR] and hole [(d) phonon-limited, (e) SR-limited, (f) phonon+SR] mobility for double-gate-like rectangular nanowire cross-section ($W_{Si} = 4$ nm, $H_{Si} = 20$ nm) for different side wall surface orientations [(001) and $(1\bar{1}0)$] and stress conditions (0 and ± 3 GP uniaxial stress along $\langle 110 \rangle$ channel direction). The symbols are obtained from the 2D k -space mobility calculator Sentaurus Band [8] assuming $H_{Si} \rightarrow \infty$. For fair comparison between the 2D and 1D quantization-based simulators, the average (rather than the effective) electric field is employed in the x-axis. In addition, consistent band-structure and scattering parameters are employed in the two simulators.

orientations, the differences in the mobility curves obtained from the two simulators are also large (see Fig. 2). Therefore, the remaining differences in the mobility curves may be caused by the 2D quantization effects. Indeed, we have checked that the differences in the mobility curves are reduced when H_{Si} is increased (not shown).

Fig. 4 (a) shows the structure of a circular nanowire transistor considered here. The simulation domain is divided into three (source, channel, and drain) sub-regions, and the DD equation (coupled with the density-gradient equation) is solved in the source/drain regions while the MSBTE is solved in the channel region. The Poisson equation is solved in the entire domain to obtain self-consistent solutions. In Figs. 4 (b)–(d), the electron density at $V_D = V_G = 0.8$ V is shown. As mentioned before, the local electron density is discontinuous at the DD/MSBTE region interface although the difference in the integrated density is only about 3%. As the

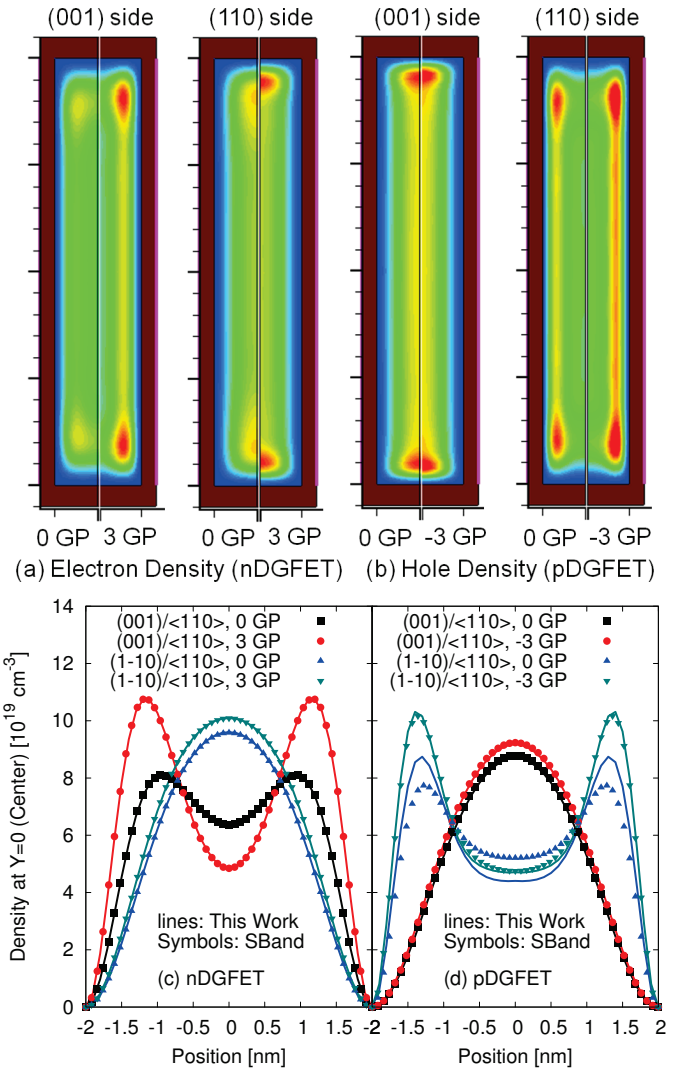


Fig. 3. 2D (a) electron and (b) hole density at the cross-section of the double-gate-like rectangular nanowire at the largest gate bias, and the corresponding 1D (c) electron and (d) hole density at $y = 0$. The symbols are obtained from the Sentaurus Band. The differences in hole density for the $[1\bar{1}0]$ orientation are due to the use of $k = 0$ wavefunction for the hole density calculation. The k -dependence is taken into account in the form factor calculation for the phonon scattering.

quantization along the side walls [$(1\bar{1}0)$ orientation] is stronger than that along the top and bottom [(001) orientation], the electron density profile in Figs. 4 (c) and (d) are anisotropic.

Fig. 5 shows the I_D - V_G curves of the n and p-type nanowire transistors without stress and with ± 3 GP uniaxial stress. The applied uniaxial stress induces significant V_T shift because of the stress-induced bandstructure changes. For the given $V_G - V_T$, the uniaxial stress enhances both the linear and saturation currents where the enhancement of the linear current is slightly larger.

The internal electron and hole density distributions as a function of position and energy in the MSBTE region can be found in Fig. 6, which clearly shows quasi-ballistic carrier transport in the channel.

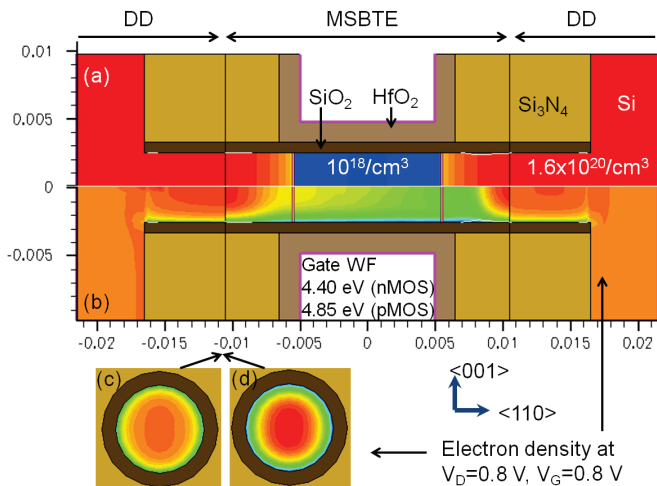


Fig. 4. (a) Doping profile and structure of a circular nanowire transistor considered in this work ($D_{\text{Si}} = 5 \text{ nm}$, $L_G = 10 \text{ nm}$), (b) electron density profile at $V_D = V_G = 0.8 \text{ V}$, (c) electron density computed from the DD equation, and (d) that from the MSBTE at the DD/MSBTE interface cross-section.

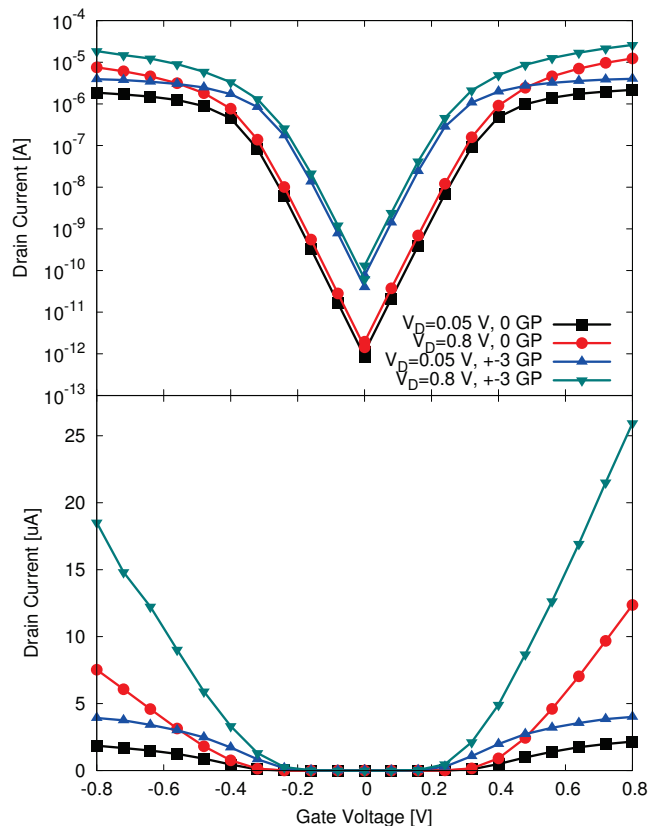


Fig. 5. I_D - V_G curves of the n and p-type nanowire transistor without stress and with $\pm 3 \text{ GP}$ uniaxial stress.

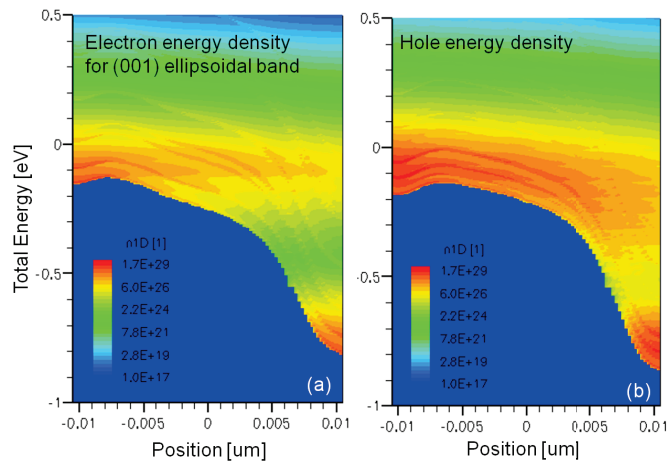


Fig. 6. (a) Electron and (b) hole density distribution as a function of position and energy when $V_D = V_G = \pm 0.8 \text{ V}$.

VI. CONCLUSION

It has been shown that the implemented coupled DD/MSBTE solver is a practical tool to study the influence of 2D quantization, quasi-ballistic carrier transport, mechanical stress, orientation, and scattering in realistic 3D multi-gate transistors with arbitrary cross-sections and realistic source/drain regions. We have also validated that the implemented 2D Schrödinger solver and the proposed surface roughness scattering model provide consistent results in the 1D quantization limit.

REFERENCES

- [1] S. Jin, M. V. Fischetti, and T.-w. Tang, "Theoretical study of carrier transport in silicon nanowire transistors based on the multisubband Boltzmann transport equation," *IEEE Trans. Electron Devices*, vol. 55, no. 11, pp. 2886–2897, 2008.
- [2] V. Sverdlov, E. Ungersboeck, H. Kosina, and S. Selberherr, "Effects of shear strain on the conduction band in silicon: An efficient two-band $k \cdot p$ theory," in *Solid State Device Research Conference, 2007. ESSDERC 2007. 37th European*. IEEE, 2007, pp. 386–389.
- [3] M. Fischetti, Z. Ren, P. Solomon, M. Yang, and K. Rim, "Six-band $k \cdot p$ calculation of the hole mobility in silicon inversion layers: Dependence on surface orientation, strain, and silicon thickness," *Journal of Applied Physics*, vol. 94, no. 2, pp. 1079–1095, 2003.
- [4] A.-T. Pham, C. Jungemann, and B. Meinerzhagen, "Physics-based modeling of hole inversion-layer mobility in strained-SiGe-on-insulator," *IEEE Trans. Electron Devices*, vol. 54, no. 9, pp. 2174–2182, 2007.
- [5] S.-M. Hong, W. Choi, W. Lee, U. Kwon, K.-H. Lee, and Y. Park, "Mobility calculation for nanoscale multi-gate FETs with arbitrary two-dimensional cross section with a homogeneous channel including strain effects," in *Intl. Conference on Simulation of Semiconductor Processes and Devices*, 2012, pp. 360–363.
- [6] M. G. Ancona and H. F. Tiersten, "Macroscopic physics of the silicon inversion layer," *Phys. Rev. B*, vol. 35, no. 15, p. 7959, May 1987.
- [7] S. Jin, M. V. Fischetti, and T.-w. Tang, "Modeling of electron mobility in gated silicon nanowires at room temperature: Surface roughness scattering, dielectric screening, and band nonparabolicity," *J. Appl. Phys.*, vol. 102, no. 8, p. 083715, Oct. 2007.
- [8] *Sentaurus Device Monte Carlo User Guide Version H-2013.03*, Synopsys, Inc., Mountain View, CA, 2013.